Thin Solid Films 669 (2019) 315–320

Contents lists available at ScienceDirect

Thin Solid Films

journal homepage: www.elsevier.com/locate/tsf

Effect of germanium incorporation on the properties of kesterite $Cu_2ZnSn(S,Se)_4$ monograins

Souhaib Oueslati[a,b,*], Maarja Grossberg[a], Marit Kauk-Kuusik[a], Valdek Mikli[a], Kaia Ernits[b], Dieter Meissner[a,b], Jüri Krustok[a,c]

[a] Department of Materials and Environmental Technology, Tallinn University of Technology, Ehitajate tee 5, 19086 Tallinn, Estonia
[b] Crystalsol OÜ, Akadeemia tee 15a, 12618 Tallinn, Estonia
[c] Divison of Physics, Tallinn University of Technology, Ehitajate tee 5, 19086 Tallinn, Estonia

ARTICLE INFO

Keywords:
Copper zinc tin sulfur selenide
Germanium
Photoluminescence
Monograin
Quantum efficiency
Current-voltage

ABSTRACT

In this work, the influence of partial substitution (up to 10%) of tin (Sn) by germanium (Ge) in $Cu_2ZnSn(S,Se)_4$ (CZTSSe) solid solution monograins was studied. The external quantum efficiency measurements of the CZTGSSe monograin layer solar cells showed an increase in the band gap energy of the Ge-substituted CZTGSSe. According to the current-voltage measurements, the higher band gap energy is accompanied with a larger open circuit voltage deficit showing the lowest value for the Ge-free sample of around 785 mV. The temperature dependent current-voltage measurements revealed strong recombination losses at the CdS/CZTGSSe interface contributing to the voltage deficit. The radiative recombination processes in CZGTSSe monograins were studied using low-temperature photoluminescence (PL) spectroscopy. A detailed analysis of the PL spectra indicates that at low temperatures the recombination of free electrons with holes localized at acceptors related to the group IV element deeper than the mean energy depth of potential fluctuations is dominating.

1. Introduction

The earth abundant kesterites $Cu_2ZnSn(S,Se)_4$ (CZTSSe) have gained much attention in materials research for solar cell application due to their suitable characteristics such as a high absorption coefficient and band gap (E_g) tunability between 1.0 eV and 1.5 eV [1]. The highest efficiency of kesterite-based solar cells of 12.6% was reached in 2013 by hydrazine-based solution produced thin film cells [2]. One of the main reasons for the lack of improvement in efficiency of CZTSSe solar cells compared to the closely related $Cu(In,Ga)Se_2$ solar cells is the recombination losses based on large open-circuit voltage (V_{OC}) deficit ($E_g/q - V_{OC}$, where q is the elementary charge) [3]. The optimization of the bandgap of the absorber by cation or anion substitution can improve the V_{OC} of the devices. One interesting approach is to substitute tin (Sn) by other cations such as germanium (Ge) leading to an increase in the bandgap [4]. The influence of Ge incorporation on the CZTSSe thin film solar cell device performance has been studied by several research groups [5–7]. Previous studies claim that the partial substitution of Sn by Ge can significantly reduce the V_{OC} deficit and lead to higher efficiency compared to the Ge-free sample [5]. Moreover, improved charge carrier collection [5] and longer minority carrier lifetime [6,7] have been reported for Ge containing CZTSSe thin film solar cells. Till now, only small quantities of Ge have led to significant improvements in the kesterite solar cell performance [8]. The beneficial effect of Ge is particularly related to processes at the absorber surface and not associated with any bulk improvement [5,8]. Giraldo et al. implemented a Ge superficial nanolayer leading to efficiency improvement from 7% to 10.1% only substituting 4% of Sn by Ge in the kesterite compound [5]. The V_{OC} increase was attributed to the formation of a liquid Ge-related phase, the possible reduction of Sn multicharge states, and the formation of GeO_x nanoinclusions. Although, Ge substitution by larger amounts (30 to 40%) has also led to small (< 1%) increase in the solar cell performance, the V_{OC} deficit has actually increased [1,6]. Those conflicting results on the effect of Ge on the performance of kesterite solar cells was the driving force for this study of the mechanisms by which the Ge could improve or deteriorate the solar cell properties.

There are only few reports in which the radiative recombination mechanisms in $Cu_2Zn(Sn_{1-x}Ge_x)(SSe)_4$ (CZGTSSe) absorber layer were investigated [1,4]. Usually, a broad asymmetric PL band is detected at low temperature and several recombination models are proposed to explain its origin. Our contribution provides an investigation of the impact of Ge incorporation into CZTSSe monograins, and its influence on the material properties and solar cell performance. A detailed

* Corresponding author at: Department of Materials and Environmental Technology, Tallinn University of Technology, Ehitajate tee 5, 19086 Tallinn, Estonia.
E-mail address: souhaib.oueslati@taltech.ee (S. Oueslati).

https://doi.org/10.1016/j.tsf.2018.11.020
Received 15 June 2018; Received in revised form 9 November 2018; Accepted 11 November 2018
Available online 13 November 2018

photoluminescence (PL) study was carried out in order to understand the role of Ge in the CZGTSSe absorber layer.

2. Experiment description

$Cu_2ZnGe_xSn_{1-x}(S_{0.8}Se_{0.2})_4$ solid solution monograins with different Ge content were prepared and studied. The amount of Sn substituted by Ge is presented as %-values of the [Ge]/([Ge] + [Sn]) atomic ratio i.e. [Ge]/([Ge] + [Sn]) atomic ratio of 0.02 is 2% of nominal Sn substitution by Ge. The contents investigated here are 0%, 2%, 4%, 6%, 8% and 10%. The Ge-free sample is the reference material. CZGTSSe materials with slightly Cu-poor ([Cu]/([Zn] + [Sn] + [Ge]) = 0.94), Zn-rich ([Zn]/([Sn] + [Ge]) = 1.03) and ([S]/([S] + [Se]) = 0.8) composition, determined by energy dispersive spectroscopy (EDX), were selected for this study. The monograin powders were synthesized at 740 °C for 88 h from elemental 5 N purity precursors: copper, zinc, tin, germanium, selenium and sulfur in molten potassium iodide (KI) in quartz ampoules. After the synthesis of the monograin powders, the flux (KI) was removed by the washing procedure at room temperature with deionized water, after which the monograin powders are dried and sieved to narrow fractions as described in detail in previous papers [9]. For monograin layer production, the desired grain sizes are 50 to 60 μm as shown in the inserted graph in Fig. 2. A monolayer of chemically and thermally treated monograins was embedded into epoxy resin. Solar cell devices were completed in a standard process using a CdS buffer layer, an i-ZnO/ZnO:Al front contact and finally applying a graphite back contact, a scheme of the monograin device structure is shown in Fig. 1. A more detailed description of the device preparation can be found elsewhere [10].

The monograins composition and quality were characterized using EDX and Raman spectroscopy, respectively. The EDX was performed in a Zeiss MERLIN scanning electron microscope operated with an accelerating voltage of 20 kV using a Röntec EDX XFlash 3001 detector. The Raman spectra were recorded by using a Horiba's LabRam HR800 spectrometer with a 532 nm laser line focused on the sample with a spot size of about 5 μm. For PL measurements, the samples were mounted in a closed-cycle He cryostat enabling variation of temperature between 10 and 300 K. The He-Cd laser 442 nm line was used as an excitation source and its intensity was attenuated with a range of neutral density filters. The PL signal was detected using a Hamamatsu InGaAs detector. For the temperature-dependent current-voltage (J-V) measurements, solar cells were mounted in a closed-cycle He cryostat. The J-V(T) curves were measured with a Keithley 2401 Source Meter under 100 mW/cm^2 illumination from a standard halogen lamp with calibrated intensity. The external quantum efficiency (EQE) measurements were performed at room temperature using chopped-light and a monochromator system from Newport.

3. Results and discussion

According to the EDX analysis of the synthesized CZGTSSe solid solution monograins, Sn is substituted with Ge by the chosen amount. Representative Raman spectra of the CZTSSe and CZGTSSe monograins are presented in Fig. 2. The Raman peaks of CZTSSe and CZGTSSe monograins are in good agreement with literature confirming the kesterite crystal structure of the formed grains [4].

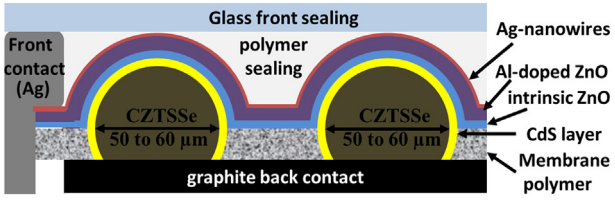

Fig. 1. Scheme of monograin solar cell structure.

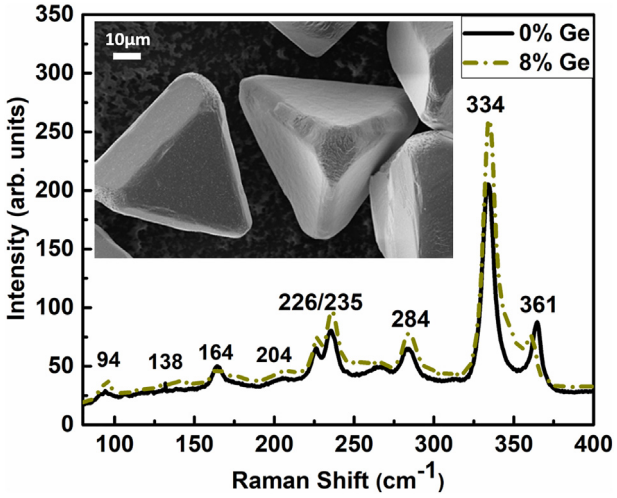

Fig. 2. Raman spectra of the CZTSSe and CZGTSSe (8% Ge) monograins. The inserted graph shows a SEM picture of the synthesized monograins with the desired size.

Current-voltage characterization of the solar cells was carried out for the reference powder and powders with different Ge content under AM1.5 illumination. The values of the open circuit voltage V_{OC}, short circuit current J_{SC}, fill factor *FF*, conversion efficiency η, band gap E_g, V_{OC} deficit of the solar cells are summarized in Table 1.

The overall power conversion efficiencies of solar cells with moderate Ge substitution of Sn (up to 4%) are roughly in the same range as for the reference device. For those devices the V_{OC} shows an increase up to 3% while the *FF* and J_{SC} remain comparable to the reference cell. On the other hand, solar cells with Ge substitution of Sn larger than 4% show a tendency to lower performance. In case of the cells with 6% and 8% Ge substitution of Sn, the V_{OC} shows higher values compared to the reference cell but with lower *FF* and J_{SC}. Sample with 10% Ge substitution of Sn shows the lowest efficiency of 5.03% due to the decrease of all the solar cell parameters.

The EQE curves are presented in Fig. 3. All devices show losses in the short wavelength region due to the absorption in the CdS buffer layer. The Ge-substituted samples show a slight enhancement on the EQE response in the short wavelength region compared to the reference cell. Although there is a trend for higher Ge content samples to better charge carrier collection in the short wavelength region, the reason for the differences between the individual samples is not completely clear.

The maximum carrier collection is observed at a wavelength of around 540 nm for all the samples and it is strictly declining on the longer wavelength region defining the material band gaps (E_g). For more precise estimation of the E_g, $(EQE*E)^2$ was plotted against the photon energy (E) and displayed as an inset graph in Fig. 3. The E_g is estimated from the interception of the linear part with the energy axis [11]. The E_g values are 1.46 ± 0.01 eV, 1.48 ± 0.01 eV, 1.50 ± 0.01 eV, 1.51 ± 0.01 eV, 1.52 ± 0.01 eV and 1.53 ± 0.01 eV for devices with 0%, 2%, 4%, 6%, 8% and 10% Ge substitution, respectively. The results are summarized in Table 1 and show an increase in E_g with increasing Ge content. The V_{OC} deficit values are calculated using the extracted E_g from the EQE data and presented in Table 1. The monotonic increase of E_g observed with increasing Ge substitution is not fully reflected in the V_{OC} parameters. While the solar cells based on Ge-substituted absorbers show higher band gap, the changes in V_{OC} are rather small and the V_{OC} deficit increases with increasing the Ge substitution. The latter behavior confirms the results reported by Bag et al. [1].

Temperature-dependent I-V measurements were performed under illumination and the thermal behavior of the relative efficiency and the V_{OC} values are shown in Fig. 4. The relative efficiencies of the devices

Table 1
Solar cell characteristics of CZGTSSe monograin devices with different Ge contents measured under AM1.5 illumination.

[Ge]/([Ge] + [Sn]) [%]	V_{OC} [V]	FF [%]	J_{SC} [mA/cm^2]	η [%]	E_g [eV]	V_{OC} deficit [V]	E_g- Φ [eV]
0%	0.675	68.5	14.2	6.56	1.46	0.785	0.17
2%	0.689	66.8	14.0	6.46	1.48	0.791	0.21
4%	0.697	69.4	14.3	6.90	1.50	0.803	0.17
6%	0.682	66.0	13.7	6.15	1.51	0.828	0.21
8%	0.695	67.1	13.0	6.08	1.52	0.825	–
10%	0.657	60.8	12.6	5.03	1.53	0.873	0.35

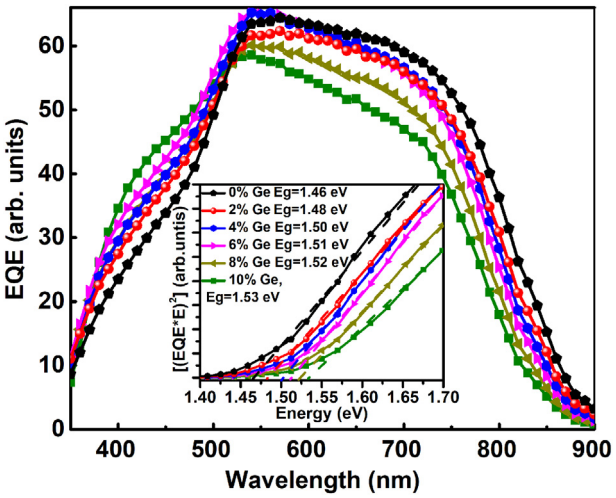

Fig. 3. EQE curves for kesterite devices with different Ge contents. The inserted graph shows the band gap extraction by plotting $[(EQE*E)^2]$ vs. E.

achieved maximum values below room temperature. The maximum efficiency for the reference device is observed at a higher temperature compared to those of the Ge-substituted devices. The decrease of $\eta(T)$ shown in Fig. 4a is mainly caused by the exponential increase of the series resistance (R_S) and the drop of the current with decreasing temperature. At low temperatures, the efficiency of the Ge-free device shows stronger dependence on temperature due to the higher R_S values at low temperatures compared to those of the Ge-substituted devices. The $FF(T)$ showed the same trend as $\eta(T)$ and even at low temperature around 20 K, FF values over 50% were observed.

The relationship between V_{OC} and temperature (T) is given as in Eq. (1):

$$V_{OC} = \frac{\Phi}{q} - \frac{Ak_BT}{q}\ln\left(\frac{J_{00}}{J_L}\right) \quad (1)$$

where Φ is the potential barrier for interface recombination, q is the elementary charge, A is the ideality factor, k_B is the Boltzmann constant, T is the temperature, J_{00} is the reverse saturation diode current prefactor and J_L is the light generated current density [12]. The V_{OC} versus T data yields to a linear behavior in the relatively high temperature region (above 200 K) as shown in Fig.4b. The extrapolation of a straight line to $T = 0K$ indicates the potential barrier Φ values for the different Ge substituted amount. The Φ values are 1.28 eV, 1.27 eV, 1.33 eV, 1.30 eV and 1.17 eV for devices with 0%, 4%, 6%, 8% and 10% Ge substitution, respectively. The significantly lower potential barrier values compared to the expected E_g values of CZGTSSe, suggest that the conduction band offset (CBO) is cliff-like which inevitably causes severe interface recombination and large V_{OC} deficit [13]. Although, the Φ values are lower than the E_g, the origin of the voltage deficit cannot solely be attributed to the interface defects and it is also affected by the bulk defects. In fact, the high defect concentration leads to band tails that reduce the effective band gap and strongly affect the V_{oc}values at room temperature [14]. Gokmen et al. suggest that the Cu and Zn

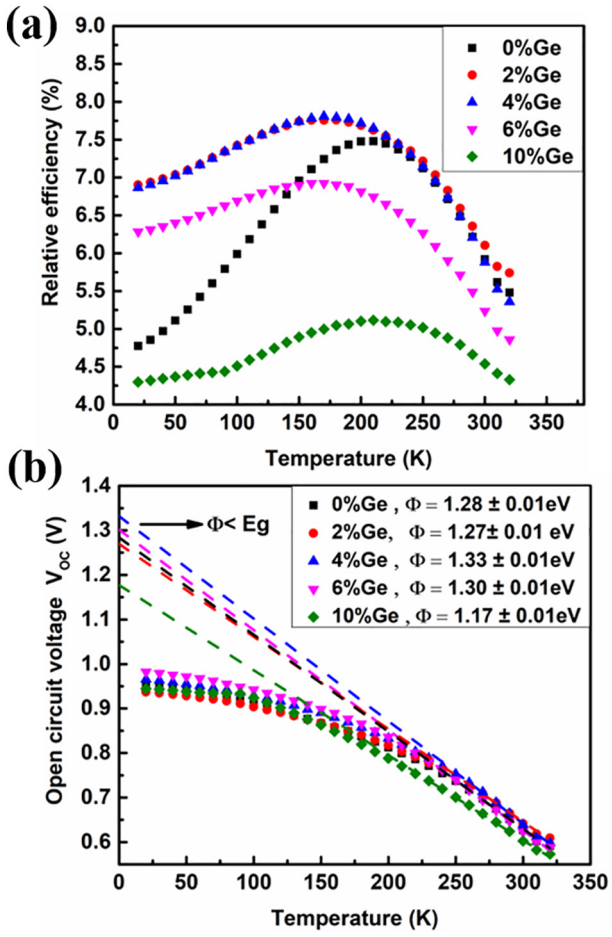

Fig. 4. (a) Temperature dependence of the efficiency of solar cells with different Ge contents, (b) Open circuit voltage V_{OC} as a function of temperature (the straight lines are linear fits according to the Eq.(1)).

randomization by antisite defect pairs [Zn_{Cu} + Cu_{Zn}] is mainly responsible for the band tails formation and increases the V_{OC} deficit [14]. However, the variation in the concentrations of Cu and Zn does not affect significantly the mean depth of the potential fluctuations in CZTSSe thin films [15] suggesting that the nature of defects which lead to the band tails requires further investigation.

Photoluminescence spectroscopy (PL) measurements offer an opportunity to study the electronic structure of semiconductors in general and in particular defect states within the band gap. Analysis of the temperature and excitation power dependent PL spectra leads to better understanding of the recombination mechanisms in kesterite monograins as well as the effect of Sn substitution by Ge on it. A detailed PL study in this work was performed on three kesterite samples (powder form) with different Ge contents of 0%, 4% and 10%. The PL spectra of the three studied powders, each of them consisting of one PL band at T = 10 K, are depicted in Fig. 5a. All three PL bands have asymmetric shape with much steeper decline on the high-energy side compared to

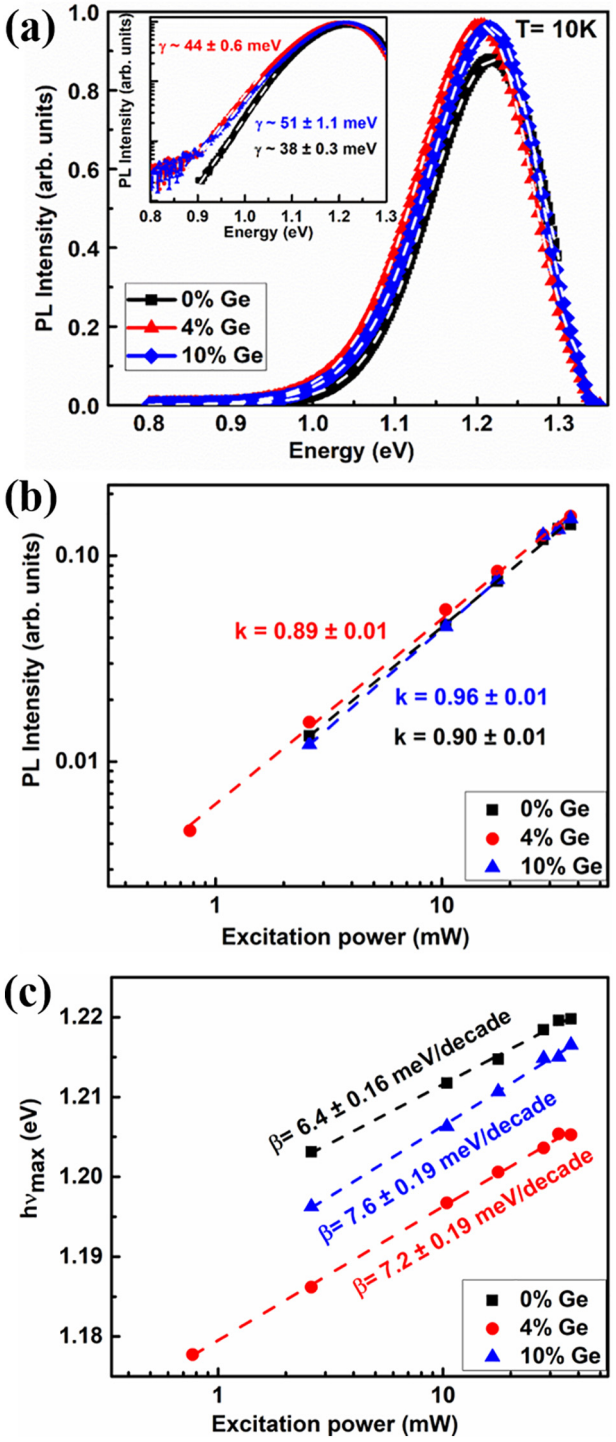

Fig. 5. (a) PL spectra of the investigated powders at T = 10 K, dashed lines show the fitting results with Eq. (2) (inset graph shows the estimation of the average depth of potential fluctuations γ), (b) dependences of the PL intensity and (c) the peak position on the excitation power at T = 10 K for CZGTSSe monograins with various Ge contents.

the low energy-side. The empirical asymmetric double sigmoidal function (DSF) proposed in [16] for bands associated with band-to-impurity (BI) recombination provides the best fitting of the PL spectra $I(h\nu)$ based on Eq. (2) and shown in Fig.5a:

$$I(h\nu) = A\left[1/\left(1+exp\left(-\frac{h\nu - E_1}{W_1}\right)\right)\right] \times \left[1 - 1/\left(1+exp\left(-\frac{h\nu - E_2}{W_2}\right)\right)\right] \quad (2)$$

where A, E_1, E_2, W_1 and W_2 are fitting parameters. There is a cut-off on the experimental spectra for energy above 1.3 eV because of the detector's limitation.

The average depth of potential fluctuations γ estimated from the low energy sides of the PL spectra [17] at T = 10 K are 38 meV, 44 meV and 51 meV for powders with 0%, 4% and 10% Ge substitution, respectively, as shown in the inset graph in Fig. 5a. The γ values show a tendency to increase as the Ge content increases.

At fixed temperature (T = 10 K), the excitation power i.e. carrier concentration dependence of the PL spectra was measured by changing the excitation power by almost three orders of magnitude. The PL intensity is related to the excitation intensity by a power law $I_{PL} \propto P_{ex}{}^{k}$, where k is the power coefficient estimated by a linear fit of the log-log plot of $I_{PL}(P_{ex})$. The fitting results are shown in Fig. 5b, the extracted slope k is 0.90, 0.89 and 0.96 for powders with 0%, 4% and 10% Ge substitution, respectively. As k is lower than unity the radiative recombination is associated with localized defects with energy levels within the band gap [18].

The PL peak positions of the three investigated powders show significant blue shifts (j-shift) with increasing the laser power as shown in Fig. 5c. The rate of the shift per decade of the laser power (β) shows tendency to increase as the Ge content increases, changing from 6.4 meV/decade for Ge-free sample to 7.2 meV/decade and 7.6 meV/decade for CZGTSSe with 4% and 10% Ge, respectively. Such a significant j-shift is a characteristic feature of a band-to-tail (BT) or a band-to-impurity (BI) transition [19] in different materials with high concentration of charged defects, where potential fluctuations starts to affect recombination processes. In fact, there are two radiative recombination pathways dominating in the kesterite materials at low temperatures: (1) the BT transition – the recombination of holes, localized in acceptor-like states of the valence band tail, with free electrons from the conduction band, and (2) the BI transition – the recombination of free electrons with holes localized in acceptor states, which are deeper than the mean energy depth of potential fluctuations [17,19]. Detailed information about recombination processes in kesterites can be found in [20].

Temperature-dependent PL of the three investigated powders was measured between 10 and 280 K under fixed excitation power density of about 500 W/cm^2. The temperature dependencies of the peak positions of the PL bands $h\nu_{max}(T)$ for the studied powders are presented in Fig. 6a showing a monotonic shift to lower energies with increasing temperature up to a characteristic temperature where a minimum value is reached. With further temperature increase, the PL peak position shifts towards higher energies. According to [19], the monotonic decrease of $h\nu_{max}(T)$ at low temperature is more rapid than the band gap shift with temperature and it may be expressed as:

$$h\nu_{max}(T) = E_g^0 + \mu_n - \sqrt{2}\gamma - \varepsilon_1 \quad (3)$$

with

$$\varepsilon_1 = k_B T \ln \frac{N_v}{p + n\theta} \quad (4)$$

where $E_g{}^0$ is the energy gap without potential fluctuations, μ_n is the Fermi energy of the electrons, N_v the effective density of states in the valence band, n and p are the concentrations of free electrons and holes, respectively, and θ is the ratio of electron and hole capture probabilities by the localized states.

The dependency of the peak position shift at low temperatures can be simplified to a linear shift. A linear fit leads to a slope α corresponding to $(\ln(N_v/p + n\theta))$ [19] which is decreasing as the Ge content increases. Slopes of 2.7, 1.9 and 1.4 were deduced for powders with 0%,

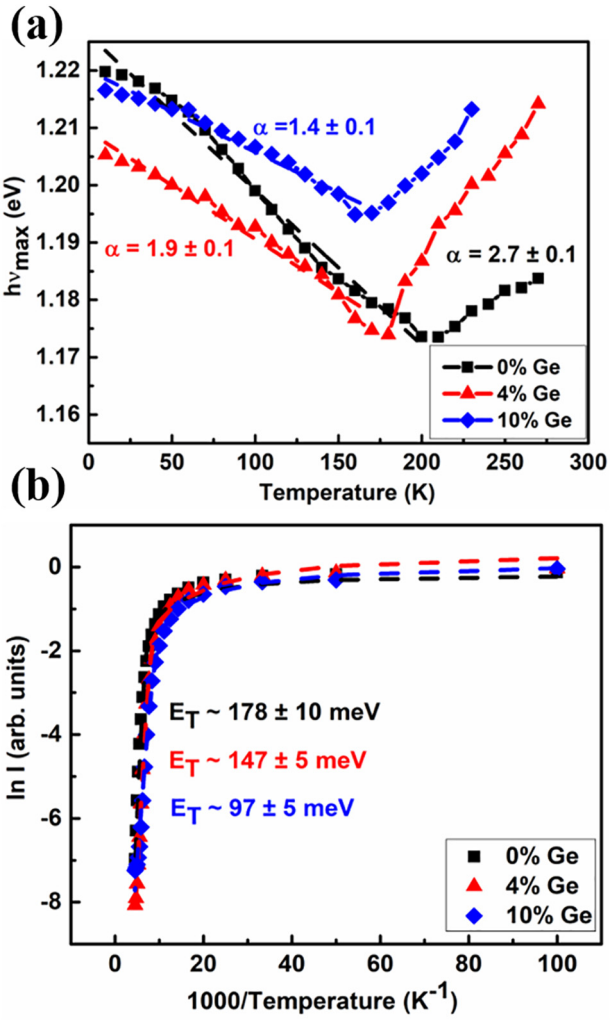

Fig. 6. (a) Temperature dependence of the peak position, (b) temperature dependence of the integrated intensities, dashed lines show the fitting results with Eq. (5).

4% and 10% Ge substitution, respectively. According to Eq. (4), lower α values correspond to higher carrier concentration ($p + n\theta$) revealing that the increase of the Ge content leads to higher carrier concentrations in the synthesized monograins. According to Eqs. (3) and (4), the $h\nu_{max}$ also shifts towards higher energies with increasing concentrations of free electrons and holes when increasing the excitation intensity, which is consistent with Fig. 5c.

The temperature dependencies of the integrated PL intensities were fitted using an Eq. (5) [21] as presented in Fig. 6b as dashed lines:

$$I(T) = I_0\,[1 + a_1 T^{3/2} + a_2 T^{3/2} exp(-E_T/k_B T)] \quad (5)$$

where $I(T)$ represents the integrated PL intensity at temperature T, I_0 is the integrated PL intensity when the temperature approaches T~ 0 K, a_1 and a_2 are fitting parameters, E_T is an activation energy and k_B is the Boltzmann constant. The thermal quenching of the PL emission can be well described by single thermal activation energy, having different values for the three studied CZGTSSe monograins. A thermal activation energy of 178 meV was found for the reference material, whereas, lower activation energies of 147 meV and 97 meV were found for materials with 4% and 10% Ge substitution, respectively.

The variation in the amount of Ge substitution of Sn affects the potential fluctuations depth and changes the thermal activation energies of the quenching of the PL emission, suggesting that the nature of involved defects can be related to the group IV elements. The formation energies of acceptor defects involving group IV elements such as Cu_{Sn} and Zn_{Sn} are high and their existence as individual defects is unlikely [22]. As a non-stoichiometric growth condition was used ([Cu]/([Zn] + [Sn]) < 1 and [Zn]/[Sn] > 1 ratio), the concentration of Zn is very high during the growth and the contributing defect cluster [Zn_{Sn} + 2Zn_{Cu}] is likely formed that induces almost negligible band edge shifts according to [22]. The Zn_{Sn} antisite involved in the latter cluster in CZTSSe monograins is partially changed to Zn_{Ge} with Ge substitution of Sn in CZGTSSe. The activation energy extracted by PL in CZTSSe monograins could be attributed to the acceptor level Zn_{Sn}, whereas in the case of CZGTSSe monograins it may be attributed to the Zn_{Sn} and Zn_{Ge} acceptor level. The tendency towards lower activation energies with increasing the Ge substitution suggests that the acceptor level in CZGTSSe is closer to the valence band leading to an increase in the p-type conductivity of the monograins. Thus, the Zn_{Sn} and Zn_{Ge} antisites concentration in CZGTSSe seems to be higher than the concentration of Zn_{Sn} in CZTSSe and the similarity of the atomic radius of Zn and Ge could increase the formation probability of Zn_{Ge} compared to Zn_{Sn}. The latter conclusion is consistent with the decrease of the slope of the PL peak position shift α with increasing the Ge substitution at low temperatures. Accordingly, the overall carrier concentration of the monograins increases with Ge substitution of Sn due to the lower activation energies or/and the higher probability of formation of Zn_{Ge} acceptor defect. The lower carrier concentration in case of Ge-free monograins explains the higher R_S values and the stronger efficiency dependence at low temperatures, observed in Fig. 4a.

The higher degree of disorder leads to a higher defect concentration in CZGTSSe monograins, which is consistent with the tendency of higher average depth of potential fluctuations γ with increasing Ge content. Since the thermal activation energies are larger than the estimated depth of potential fluctuations, the PL spectra at low temperatures are likely related to BI transitions and treated as a recombination of free electrons from the Fermi level with a hole captured by a localized acceptor level Zn_{Sn} or Zn_{Sn} and Zn_{Ge}.

4. Conclusions

We show that one way to increase the band gap and the p-type conductivity of CZTSSe kesterite material is through the partial substitution of Sn by Ge. The higher p-type conductivity of CZGTSSe could explain the slower decrease of the performance of the Ge-substituted devices at low temperatures compared to the reference device. The partial substitution of Sn by Ge in the solid solution case increases the degree of cationic disorder and leads to higher defect concentration and band gap fluctuations causing band tailing. The Ge substitution of Sn by the amount used in this study (up to 10%) did not change the dominating radiative recombination mechanism involving deep acceptor defects related to the group IV elements deeper than the mean energy depth of potential fluctuations in the CZGTSSe monograins. Recombination involving deep defects in the bulk of these kesterites together with the observed interface recombination in all studied CZGTSSe monograin solar cells with different Ge contents contributes to the large open circuit voltage deficit of the CZGTSSe monograin solar cells.

Acknowledgements

This work was supported by Institutional research funding IUT19-28 of the Estonian Ministry of Education and Research and by the European Union through the European Regional Development Fund, Projects TK141 and MOBJD308.

References

[1] S. Bag, O. Gunawan, T. Gokmen, Y. Zhu, D.B. Mitzi, Hydrazine-processed Ge-substituted CZTSe solar cells, Chem. Mater. 24 (2012) 4588.

[2] D.A.R. Barkhouse, O. Gunawan, T. Gokmen, T.K. Todorov, D.B. Mitzi, Device characteristics of a 10.1% hydrazine-processed $Cu_2ZnSn(Se,S)_4$ solar cell, Prog. Photovolt. Res. Appl. 20 (2012) 6.
[3] J. Kim, S. Park, S. Ryu, J. Oh, B. Shin, Improving the open-circuit voltage of $Cu_2ZnSnSe_4$ thin film solar cells via interface passivation, Prog. Photovolt. Res. Appl. 25 (2017) 308–317.
[4] M. Grossberg, K. Timmo, T. Raadik, E. Kärber, V. Mikli, J. Krustok, Study of structural and optoelectronic properties of $Cu_2Zn(Sn_{1-x}Gex)Se_4$ (x = 0 to 1) alloy compounds, Thin Solid Films 582 (2015) 176–179.
[5] S. Giraldo, M. Neuschitzer, T. Thersleff, S. López-Marino, Y. Sánchez, H. Xie, M. Colina, M. Placidi, P. Pistor, V. Izquierdo-Roca, K. Leifer, A. Pérez-Rodríguez, E. Saucedo, Large efficiency improvement in $Cu_2ZnSnSe_4$ solar cells by introducing a superficial Ge nanolayer, Adv. Energy Mater. 5 (2015) 1501070.
[6] C.J. Hages, S. Levcenco, C.K. Miskin, J.H. Alsmeier, D. Abouras, R.G. Wilks, M. Bar, T. Unold, R. Agrawal, Improved performance of Ge-alloyed CZTGeSSe Thin-film solar cells through control of elemental losses, Prog. Photovolt. Res. Appl. 23 (2015) 376–384.
[7] S. Kim, K.M. Kim, H. Tampo, H. Shibata, S. Niki, Improvement of voltage deficit of Ge-incorporated kesterite solar cell with 12.3% conversion efficiency, Appl. Phys. Express 9 (2016) 102301.
[8] M. Neuschitzer, M.E. Rodriguez, M. Guc, J. Marquez, S. Giraldo, I. Forbes, A. Perez-Rodriguez, E. Saucedo, Revealing the beneficial effects of Ge doping on $Cu_2ZnSnSe_4$ thin film solar cells, J. Mater. Chem. A 6 (2018) 11759–11772, https://doi.org/10.1039/C8TA02551G.
[9] M. Kauk-Kuusik, X. Li, M. Pilvet, K. Timmo, M. Grossberg, T. Raadik, M. Danilson, V. Mikli, M. Altosaar, J. Krustok, J. Raudoja, Study of $Cu_2CdGeSe_4$ monograin powders synthesized by molten salt method for photovoltaic applications, Thin Solid Films 666 (2018) 15–19.
[10] C. Neubauer, A. Samieipour, S. Oueslati, K. Ernits, D. Meissner, Spatially resolved opto-electrical performance investigations of $Cu_2ZnSnS_{3.2}Se_{0.8}$ photovoltaic devices, Energy Sci. Eng. 6 (2018) 563–569.
[11] R. Klenk, H.W. Schock, W.H. Bloss, Photocurrent collection in thin film solar cells calculation and characterization for $CuGaSe_2$/(Zn,Cd)S, Proc. of the 12th EU PVSEC, 1994, p. 1588.
[12] J. Li, D. Wang, X. Li, Y. Zeng, Y. Zhang, Cation Substitution in Earth-Abundant kesterite Photovoltaic Materials, Adv. Sci. 5 (2018) 1700744.
[13] S. Oueslati, G. Brammertz, M. Buffière, H. Elanzeery, O. Touayar, C. Köble, J. Bekaert, M. Meuris, J. Poortmans, Physical and electrical characterization of high-performance $Cu_2ZnSnSe_4$ based thin film solar cells, Thin Solid Films 582 (2015) 224–228.
[14] T. Gokmen, O. Gunawan, T.K. Todorov, D.B. Mitzi, Band tailing and efficiency limitation in kesterite solar cells, Appl. Phys. Lett. 103 (2013) 103506.
[15] M. Lang, T. Renz, N. Mathes, M. Neuwirth, T. Schnabel, H. Kalt, M. Hetterich, Influence of the Cu Content in $Cu_2ZnSn(S,Se)_4$ solar cell absorbers on order-disorder related band gap changes, Appl. Phys. Lett. 109 (2016) 142103.
[16] M.V. Yakusheva, M.A. Sulimov, J. Márquez-Prieto, I. Forbes, J. Krustok, P.R. Edwards, V.D. Zhivulko, O.M. Borodavchenko, A.V. Mudryi, R.W. Martin, Influence of the copper content on the optical properties of CZTSe thin films, Sol. Energy Mater. Sol. Cells 168 (2017) 69–77.
[17] A.P. Levanyuk, V.V. Osipov, Edge luminescence of direct-gap semiconductors, Sov. Phys. Usp. 24 (1981) 187–215.
[18] S. Oueslati, G. Brammertz, M. Buffière, C. Köble, T. Oualid, M. Meuris, J. Poortmans, Photoluminescence study and observation of unusual optical transitions in $Cu_2ZnSnSe_4$/CdS/ZnO solar cells, Sol. Energy Mater. Sol. Cells 134 (2015) 340–345.
[19] J. Krustok, J. Raudoja, M. Yakushev, R.D. Pilkington, H. Collan, On the shape of the close-to-band-edge photoluminescent emission spectrum in compensated $CuGaSe_2$, Phys. Status Solidi (a) 173 (1999) 483.
[20] M. Grossberg, J. Krustok, J. Raudoja, K. Timmo, M. Altosaar, T. Raadik, Photoluminescence and Raman study of $Cu_2ZnSn(Se_xS_{1-x})_4$ monograins for photovoltaic applications, Thin Solid Films 519 (2011) 7403–7406.
[21] J. Krustok, H. Collan, K. Hjelt, Does the low temperature Arrhenius plot of the photoluminescence intensity in CdTe point towards an erroneous activation energy? J. Appl. Phys. 81 (1997) 1442.
[22] S. Chen, A. Walsh, X. Gong, S. Wei, Classification of Lattice Defects in the kesterite Cu_2ZnSnS_4 and $Cu_2ZnSnSe_4$ Earth-Abundant Solar Cell Absorbers, Adv. Mater. 25 (2013) 1522–1539.